

PERSPECTIVE

Kralchevsky *et al.*
 The colloid structural forces as a tool for particle characterization and control of dispersion stability

ARTICLE

Johnston, Posada-Amarillas *et al.*
 Structures and energetics of 98 atom Pd–Pt nanoalloys: potential stability of the Leary tetrahedron for bimetallic nanoparticles

The colloid structural forces as a tool for particle characterization and control of dispersion stability†

Elka S. Basheva,^a Peter A. Kralchevsky,^{*a} Krassimir D. Danov,^a Kavssery P. Ananthpadmanabhan^b and Alex Lips^b

Received 16th April 2007, Accepted 8th June 2007

First published as an Advance Article on the web 5th July 2007

DOI: 10.1039/b705758j

Knowing the size and interactions of colloid particles, one can predict the stepwise thickness transitions and the contact angles of particle-containing liquid films. Here, we consider the inverse problem, *viz.* how to determine the particle properties by measurements with liquid films. We carried out experiments with films formed from aqueous solutions of two nonionic surfactants, Brij 35 and Tween 20, which contain spherical micelles of diameters in the range 7–9 nm. From the measured contact angles, we determined the micelle aggregation number and volume fraction. In addition, from the measured disjoining-pressure isotherms we determined the micelle diameter. In other words, the liquid-film measurements give information about the micelles, which is analogous to that obtainable by dynamic and static light scattering. Furthermore, we investigate the predictions of different quantitative criteria for stability–instability transitions, having in mind that the oscillatory forces exhibit both maxima, which play the role of barriers to coagulation, and minima that could produce flocculation or coalescence in colloidal dispersions (emulsions, foams, suspensions). The interplay of the oscillatory force with the van der Waals surface force is taken into account. Two different kinetic criteria are considered, which give similar and physically reasonable results about the stability–instability transitions. Diagrams are constructed, which show the values of the micelle volume fraction, for which the oscillatory barriers can prevent the particles from coming into close contact, or for which a strong flocculation in the depletion minimum or a weak flocculation in the first oscillatory minimum could be observed.



Elka S. Basheva took her MSc degree from the Faculty of Chemistry, University of Sofia in 1976. Since 1983 she has been Research Associate and Senior Research Associate in the Laboratory of Chemical Physics and Engineering in the same faculty. She is author of about 15 papers published in international scientific journals. Her research interests are in the field of experiments with

foam and emulsion films: thin-film-pressure balance; surface forces; role of surfactants as foam stabilizers and boosters, and food emulsions stabilized by proteins.

^a Laboratory of Chemical Physics & Engineering, Faculty of Chemistry, University of Sofia, Sofia, 1164, Bulgaria. E-mail: pk@lcpe.uni-sofia.bg; Fax: (+359) 2-962 5643; Tel: (+359) 2-962 5310

^b Unilever Research & Development, Trumbull, Connecticut, 06611, USA

† The HTML version of this article has been enhanced with colour images.

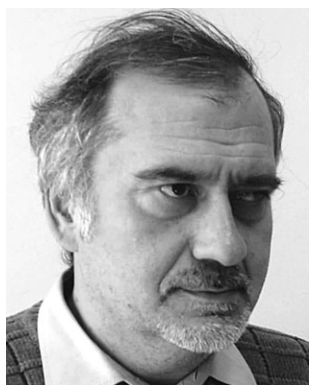
1 Introduction

Oscillatory structural forces appear when monodisperse spherical (in some cases ellipsoidal or cylindrical) particles are confined between the two surfaces of a thin liquid film.¹ Even one “hard wall” can induce ordering among the neighbouring molecules of the liquid. The oscillatory structural force is a result of the overlap of the structured zones formed in the



Peter A. Kralchevsky was born in 1956 in Gabrovo, Bulgaria. He took his MSc degree from the Department of Theoretical Physics (1981), and PhD—from the Faculty of Chemistry (1985) at the University of Sofia, where he is now full professor at the Laboratory of Chemical Physics and Engineering. He is author of about 150 papers in international scientific journals in the field of colloid

science: particles at interfaces; capillary and surface forces; adsorption from surfactant solutions; micellization and solubilization; foams, and emulsions.



Krassimir D. Danov was born in 1956 in Pleven, Bulgaria. He took his PhD degree at the University of Sofia in 1985. Now, he is a full professor of Mathematical Modeling and Applied Mathematics at the Faculty of Chemistry, University of Sofia. He is author of about 135 papers published in international scientific journals, concerning hydrodynamics of liquid films, drops and bubbles; surfactant adsorption; micellization; bulk and interfacial rheology; hydrodynamic instabilities; interactions between colloidal particles; flocculation dynamics.



Kavssery P. Ananthapadmanabhan (Ananth) was born in Kerala, India in 1952. He received his BTech degree from the Indian Institute of Technology, Mumbai, India and his Masters (1976) and Doctorate (1980) from Columbia University in New York. He was a member of the Surface Chemistry Skill Center of Union Carbide Corporation from 1983 to 1990. He joined Unilever R&D in 1990 where he is

now a lead scientist leading a group on surfactants and polymers. His research interests include surfactant solution chemistry, surfactant interactions with polymers, proteins, bio-membranes and skin.



Alex Lips was born in Austria in 1946. He received his BSc degree in chemistry from Imperial College, London, in 1968, and he embarked on his long career in Unilever Research in that year. In 1974, he received his PhD degree in Colloidal Light Scattering. He has been researching in a wide range of areas concerning home and personal care as well as foods.

His research interests include colloidal optics and rheology, surfactants, polymers and emulsions. He currently is the Director of Materials Science at the Unilever R&D facility in Trumbull, CT.

vicinity of each of the two film surfaces.² It was first detected by means of a surface-force apparatus in organic liquids^{3,4} and in aqueous solutions^{2,5} confined between two smooth solid surfaces. In this case, the oscillatory forces are often called the

solvation or hydration forces, and their period is of the order of the molecular diameter.

Oscillatory forces are observed also when spherical colloidal particles are confined in a liquid film (colloid structural forces). The phenomenon step-wise thinning or “stratification” of foam films, which was discovered long ago,^{6,7} was explained by the action of oscillatory structural forces due to the presence of surfactant micelles or latex particles in such films.^{8–13} The stable branches of the oscillatory curves have been detected by means of a thin-film-pressure balance.^{14,15} Oscillatory forces due to surfactant micelles and microemulsion droplets have been measured also by means of a surface-force apparatus,^{16,17} by atomic force microscopy,¹⁸ by light-scattering method,¹⁹ in asymmetric films,²⁰ in emulsion films,²¹ and in films containing solid colloidal spheres.^{8,9,22–24} Such forces are observed also in more complex systems like protein solutions, surfactant–polymer mixtures, and ABA amphiphilic block copolymers.^{25–33} At lower particle concentrations the structural force degenerates into the so-called depletion attraction, which is found to destabilize various dispersions.^{2,34}

The *direct* theoretical problem consists in calculating the oscillatory force at known particle size and concentration. The developed theories are based on modelling by means of the integral equations of statistical mechanics^{35–39} and numerical simulations.^{40–43} As a rule, these approaches are related to complicated theoretical expressions or numerical procedures, in contrast with the Derjaguin–Landau–Verwey–Overbeek (DLVO) theory, one of its main advantages being its simplicity.² To overcome this difficulty, some relatively simple semiempirical expressions have been proposed^{44,45} on the basis of fits of theoretical results for hard-sphere fluids.

The *inverse* theoretical problem consists in determining the particle size and concentration from the measured oscillatory force or related parameters, such as step-wise transitions in the thickness of liquid films or their contact angles. In particular, the thickness transitions are sensitive to the particle *diameter*, whereas the contact angles of the thin liquid films are sensitive to the osmotic pressure of the particles in the surrounding bulk liquid, *i.e.* to the particle *bulk concentration*.

Here, we consider the key issue about the quantitative comparison of theory and experiment, and to demonstrate what information (and how) could be extracted by data analysis. For this goal, we need a quantitative theoretical model, which is based on analytical expressions for the oscillatory structural force. (The alternative numerical simulation methods, “Monte Carlo” and “Molecular Dynamics”, are not suitable for incorporations in programs for data processing.) Accurate analytical expressions for the structural force are available only for systems of *hard spheres*; see Section 4. Correspondingly, the main reason to work with nonionic surfactants in our experiments (Section 2) is that the nonionic micelles can be adequately described as hard spheres. Well-pronounced stratification is observed also with films containing micelles of ionic surfactants.^{8–11,14–16} Unfortunately, for charged particles (including ionic micelles) accurate analytical expressions for the structural force have not yet been obtained.

Thus, our first goal in the present study is to determine (i) the diameter and (ii) aggregation number of nonionic surfactant micelles by measurements with thin liquid films. From the

measured film-thickness transitions, we determine the micelle diameter (instead of dynamic light scattering, DLS). From the measured contact angle we determine the micelle aggregation number (instead of static light scattering, SLS). An advantage of this approach is that the micelle aggregation number and volume fraction can be determined for each given concentration. It is not necessary to assume that the micelle aggregation number is independent of surfactant concentration, as when applying SLS with Zimm plot (method of double extrapolation).^{46,47}

Our second goal is to determine under what conditions the surfactant micelles produce stabilizing or destabilizing effect on colloidal dispersions (emulsions, foams, suspensions). Indeed, the oscillatory forces exhibit both maxima, which play the role of barriers to coagulation, and minima that could produce particle flocculation. So, it is important to find a quantitative criterion, which would allow one to determine which of these two opposite tendencies prevails under given experimental conditions. Because the present study is restricted to nonionic systems, we investigate the interplay of the oscillatory structural forces with the van der Waals surface forces.

2 Experimental section

2.1 Materials

In our experiments, we used micellar solutions of two nonionic surfactants. The first of them is Brij 35, C₁₂H₂₅(OCH₂CH₂)₂₃OH, a dodecyl-poly(ethylene oxide)-ether (Sigma-Aldrich); molecular weight 1198 g mol⁻¹; critical micelle concentration (CMC) = 9 × 10⁻⁵ M.^{48–50} For Brij 35, literature data are available about the micelle diameter, *d*, and aggregation number, *N*_{agg} (see Section 5.1). In some of the experiments, we added NaCl (Merck) to the solutions of Brij 35 to check whether the stepwise transitions in the film thickness are affected by electrostatic effects.⁵¹

The second used nonionic surfactant was Tween 20, C₅₈H₁₁₄O₂₆-polyoxyethylene 20-sorbitan monolaurate (Product of Fisher Chemicals, Enzyme grade). The structural formula of this surfactant is shown in Fig. 1. Note that the values of the parameters *w*, *x*, *y* and *z* (Fig. 1), as well as the micelle size and aggregation number, could be different for different samples of Tween 20. To characterize our sample, we carried out dynamic light scattering experiments (Malvern Instrument 4700C, UK, with argon laser of wavelength 488 nm.) The obtained micelle size distribution is shown in Fig. 2. The mean micelle diameter is *d* = 7.2 nm with standard deviation of the log-normal distribution σ_d = 1.2 nm. The

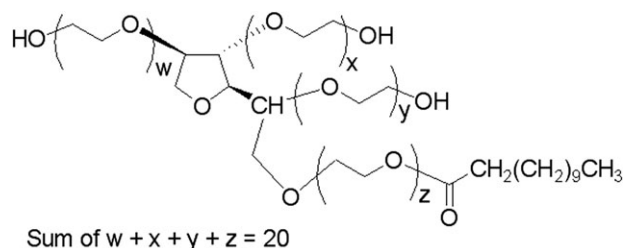


Fig. 1 The structural formula of Tween 20, C₅₈H₁₁₄O₂₆-Polyoxyethylene 20-Sorbitan Monolaurate (from Sigma-Aldrich).

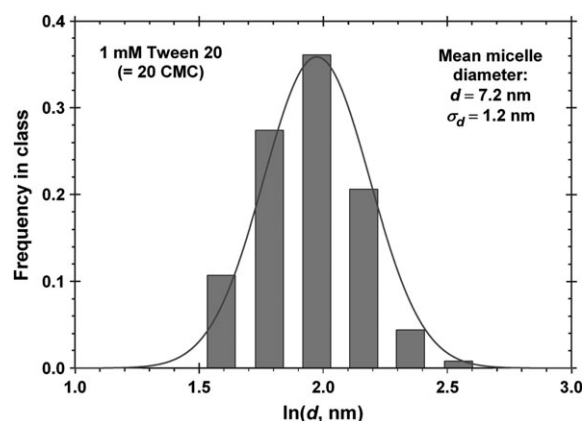


Fig. 2 Size distribution of the micelles of Tween 20 obtained by dynamic light scattering. The solid line is fit by log-normal distribution. The mean micelle diameter is *d* = 7.2 nm; the standard deviation is σ_d = 1.2 nm.

critical micelle concentration (CMC) of Tween 20 is 1.1 × 10⁻⁶ M, and its surface tension at CMC is σ = 40 ± 0.1 mN m⁻¹.⁵²

The working temperature was 25 °C in all experiments. Pure deionized water (Millipore setup) was used. The working solutions were prepared by dilution of a concentrated stock solution a day before the experiments and stored at room temperature in closed vessels.

2.2 Methods

The foam films were studied by using two different methods: the capillary cell by Scheludko and Exerowa^{53,54} (Fig. 3(a)), and the porous-plate cell by Mysels and Jones⁵⁵ (Fig. 3(b)). The former method was applied for interferometric measurements of the equilibrium film thickness at constant capillary pressure. This method gives the variation of the film thickness with time, *H*_f = *H*_f(*t*), and allows contact-angle measurements. Microscopic films of radius about 150 μm, formed in a glass ring of inner radius *R*_c = 1 mm, were studied. The capillary pressure (*P*_c = 2σ/*R*_c) was about 80 Pa in these experiments.

The Mysels–Jones⁵⁵ porous plate cell (Fig. 3(b)) was used for measuring disjoining pressure vs. film thickness isotherms, Π(*H*_f), see also ref. 14. (The disjoining pressure equals the surface force per unit area of the film.) A detailed description of the used experimental cell and procedure is presented in ref. 56. This method allows one to perform experiments at higher capillary pressures, because the radii of the pores of the film holder are much smaller than the radius of the sucking capillary in the Scheludko method.^{53,54}

Film thickness measurements. For both experimental cells, the film thickness, *H*_f, was determined from the measured intensity, *I*, of the reflected monochromatic light:⁵⁷

$$H_f = \frac{\lambda}{2\pi n_f} \left(j\pi \pm \arcsin \sqrt{\frac{I - I_{\min}}{I_{\max} - I_{\min}}} \right) \quad (1)$$

where *I*_{max} and *I*_{min} denote the maximal and minimal intensity of the reflected light; *j* = 0, 1, 2, ... is the order of the interference maxima, λ is the wavelength of the used

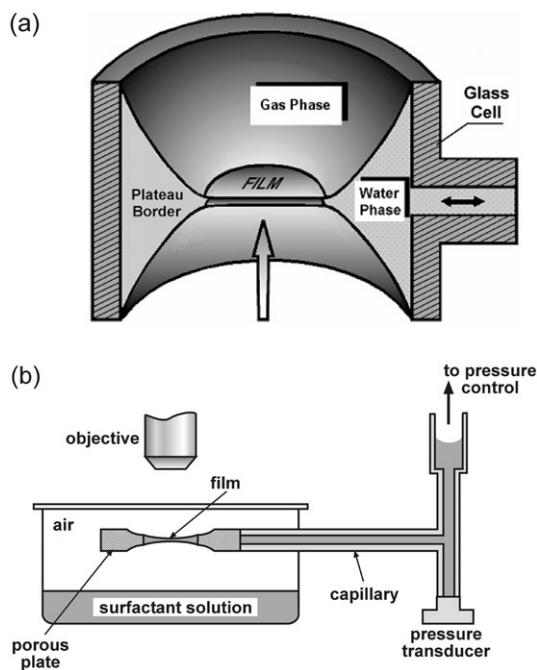


Fig. 3 Sketch of the experimental cells for investigation of liquid films. (a) Capillary cell.^{53,54} First, the cylindrical glass cell is filled with the working liquid (e.g. water solution); next, a portion of the liquid is sucked out from the cell through the orifice in the glass wall. In the central part of the cell, a liquid film is formed, which is encircled by a Plateau border. The arrow denotes the direction of illumination and microscope observation. (b) Porous-plate cell.⁵⁵ The working solution is supplied to a ring of porous glass. The pressure jump is achieved by sucking liquid; its variation enables one to measure the disjoining-pressure isotherm of the film.

monochromatic light (546 nm in our case), and n_f is the refractive index of the liquid forming the film. A photomultiplier tube was employed to determine the intensity of the reflected light with a sufficiently high precision. The film thickness, H_f , was calculated with maximum uncertainty of

about ± 1 nm. The value of H_f obtained by substituting the refractive index of water ($n_f = 1.333$) in eqn (1) is called “equivalent water thickness”. It is very close to the real film thickness when the refractive index in the zone of the surfactant paraffin tails is close to that of water. This is fulfilled in our case because we are dealing with dense (saturated) adsorption layers, which are typical at surfactant concentrations around and above the CMC.

Contact angle measurements. These measurements were carried out by means of the capillary cell (Fig. 3(a)). The contact angle, α , which (by definition) is the half of the angle subtended between the two meniscus surfaces at the periphery of the film, was found from the positions of the Newton interference rings around the film periphery (see Fig. 4). Bright and dark rings (due to constructive and destructive interference) correspond to local distances between the two menisci equal to $m\lambda/(4n_f)$, $m = 1, 2, 3, \dots$; $m = 1$ for the first (inner) bright ring. In general, the bright rings correspond to odd m , while the dark rings—to even m ; $\lambda = 546$ nm in our experiments. By means of a computer program, we fitted the observed ring locations with the numerical solution of the Laplace equation of capillarity, and determined the contact angle from the fits; see ref. 58 for details. The accuracy of the interferometrically determined contact angle is typically within $\pm 0.1^\circ$.

Disjoining pressure measurements. Disjoining pressure isotherms, $\Pi(H_f)$, were measured with a thin-film-pressure balance, using a modified version⁵⁶ of the porous-plate cell.⁵⁵ The film is formed by sucking liquid (rather than by compression of the gas phase); the cell is directly connected to a pressure transducer, the reference pressure being the atmospheric one (Fig. 3(b)). This configuration provides the opportunity to investigate both foam and emulsion films. In our experiments, the glass plate has pores of 8 μm average diameter. The cylindrical hole, where the films are formed, has a diameter of 1 mm. For each value of the applied pressure, Π , the film thickness, H_f , is determined interferometrically; see eqn (1).

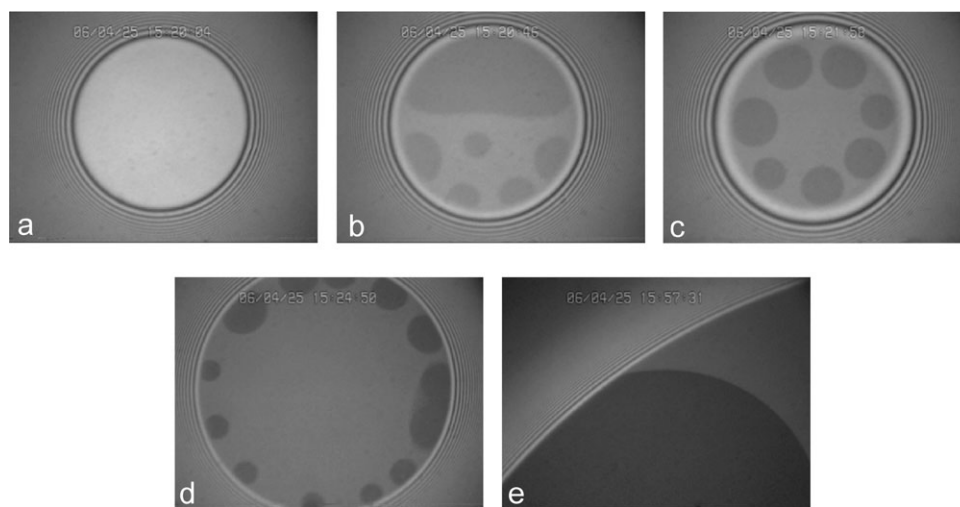


Fig. 4 Consecutive stages of the step-wise thinning of a liquid film formed from a solution of 0.1 M Brij 35 + 0.1 M NaCl. (a) Film with four micelle layers. Transitions to films with (b) three, (c) two and (d) one micelle layers. (e) Transition to a sterically stabilized Newton black film that does not contain micelles.

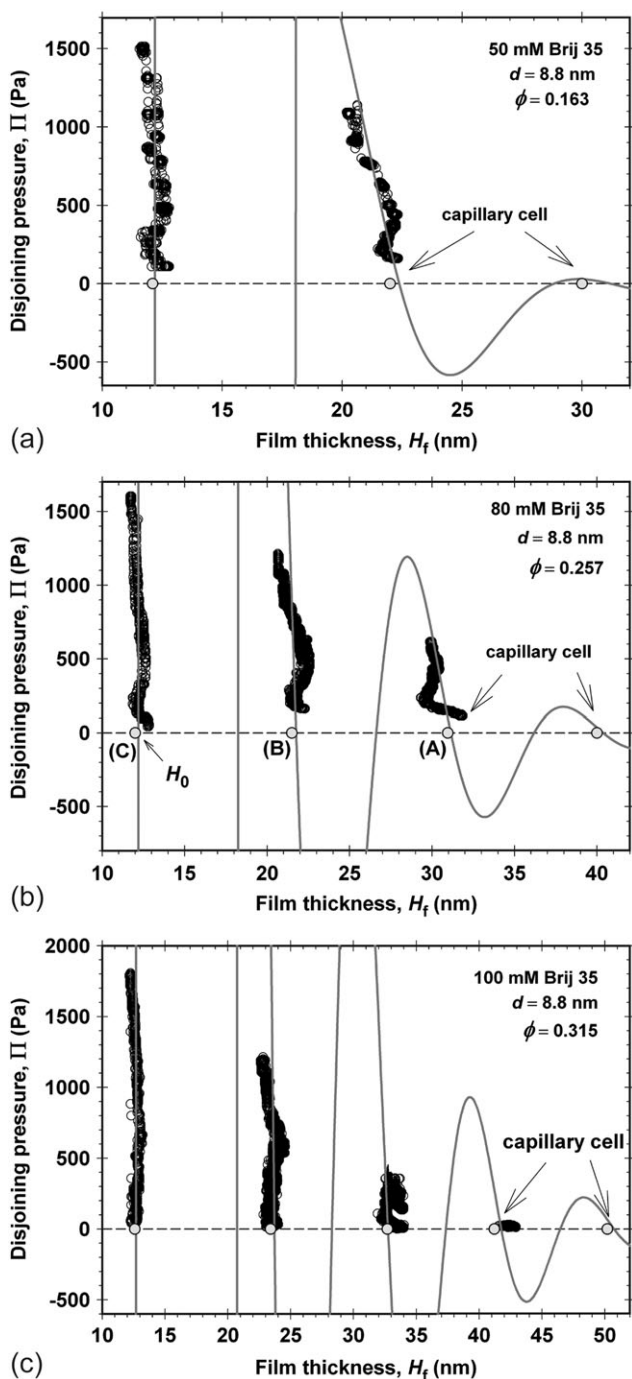


Fig. 5 Disjoining pressure, Π , vs. film thickness, H_f , measured by the porous-plate cell (Fig. 3(b)). (a) 50 mM Brij 35; (b) 80 mM Brij 35; (c) 100 mM Brij 35. The points on the horizontal axis denote the respective values of H_f for the steps measured by the capillary cell (Fig. 3(a)). The solid line shows the best fit of the $\Pi(H_f)$ dependence by means of eqn (7), which corresponds to micelle diameter, d , and volume fraction, ϕ , denoted in the figure.

3 Experimental results

Fig. 4 shows photographs of the process of thinning of a foam film formed in the capillary cell (Fig. 3(a)) from a solution of 0.1 M Brij 35 + 0.1 M NaCl. The stepwise diminishing of the film thickness (stratification) occurs through formation and

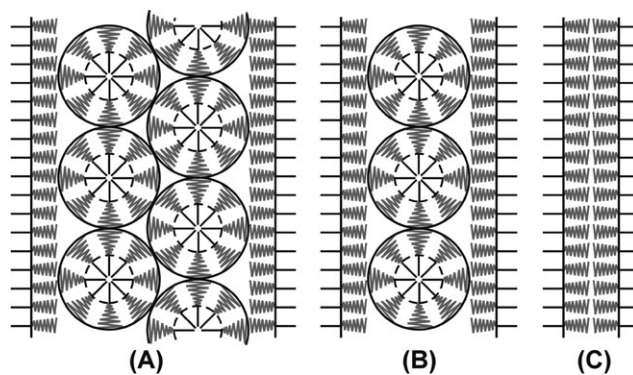


Fig. 6 The experimental repulsive portions of the $\Pi(H_f)$ isotherm, for example, at $H_f \approx 32, 22$ and 12 nm in Fig. 5(b), can be identified with (meta)stable films containing, respectively, (A) two, (B) one, and (C) zero micelle layers. In the latter case (C) the film is stabilized by the steric repulsion between the polyoxyethylene chains of the two surfactant adsorption layers.

expansion of spots of smaller thickness in the film. Each metastable state of a given uniform thickness corresponds to a given number of micelle layers within the film.⁸ In reflected light, the films look grey; the thinner films look darker. The final stable state corresponds to a Newton black film (Fig. 4(e)) of thickness $H_0 \approx 12$ nm (Fig. 5), which does not contain micelles and is stabilized by the steric repulsion between the ethylene-oxide chains of the two surfactant adsorption monolayers (Fig. 6(C)).

Fig. 5 shows plots of disjoining pressure, Π , vs. the film thickness, H_f , for foam films formed from solutions of 50, 80 and 100 mM Brij 35, obtained by means of the porous-plate cell (Fig. 3(b)). The number of the observed stepwise transitions in the film thickness increases with the rise of the surfactant concentration (compare the curves in Fig. 5(a), (b) and (c)). The addition of 0.1 M NaCl in some experiments did not produce any noticeable effect on the observed stratification. The experimental repulsive portions of the $\Pi(H_f)$ isotherm at $H_f \approx 32, 22$ and 12 nm, can be identified with (meta)stable films containing, respectively, two, one and zero micelle layers (Fig. 6). The theoretical lines are drawn by means of the procedure from Section 4.2. The circles on the horizontal axis (Fig. 5) denote the experimental values of H_f for the states of uniform thickness observed in the capillary-cell (Fig. 3(a) and 4). Because of the lower applied pressure, in the capillary cell one could observe transitions of higher order, which are not observable in the porous-plate cell.

It should be noted that the explanation of the stepwise transitions in the film thickness as a layer-by-layer thinning of an ordered structure of spherical micelles within the film (Fig. 6) was first given by Nikolov *et al.*^{8–10} (Before that it was believed that the stepwise transitions are due to the formation of a lamella-liquid-crystal structures of surfactant molecules in the films.) One of the direct proofs was given by Denkov *et al.*,^{59,60} who succeeded in freezing foam films at various stages of stratification. The electron microscope pictures of such vitrified stratifying films containing latex particles (144 nm in diameter) and bacteriorhodopsin vesicles (44 nm in diameter) showed ordered particle arrays of hexagonal packing.⁶⁰

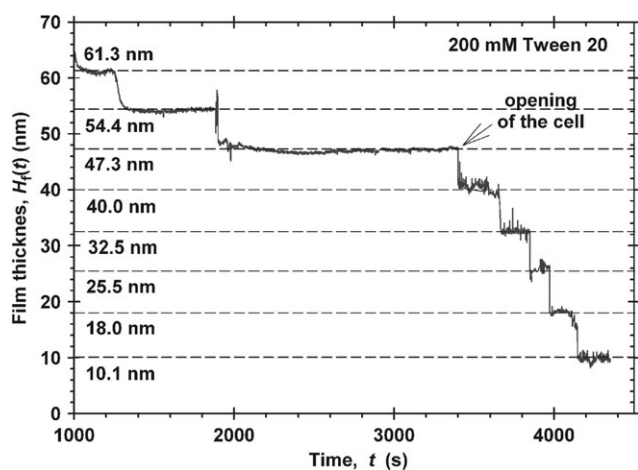


Fig. 7 Experimental dependence of the film thickness, H_f , on time, t , for a foam film formed in the capillary cell (Fig. 3(a)) from a 200 mM aqueous solution of Tween 20. To provoke the last five stepwise transitions, each time the cell was opened for a while to cause evaporation-driven increase of the driving pressure. The horizontal lines correspond to the best fit of the data (Section 4.2).

Fig. 7 shows an experimental curve obtained by means of the capillary cell (Fig. 3(a)) for a solution containing 200 mM Tween 20. The first two stepwise transitions happen spontaneously. The next five stepwise transitions could be observed only if the driving capillary pressure is increased. This is achieved by opening the cover of the experimental cell for a while to allow evaporation from the film. The hydrodynamic flow that compensates the evaporated water gives rise to a considerable pressure difference between the film centre and periphery that forces the occurrence of the last stepwise transitions; see eqn (14.22) in ref. 61. After occurrence of each transition, the cell was closed again to measure the film thickness. This procedure was repeated five times to provoke the last five transitions in Fig. 7. The average height of a step is 7.2 nm, which coincides with the micelle diameter measured by DLS (Fig. 2).

Fig. 8 shows the dependence of disjoining pressure, Π , on the film thickness, H_f , measured by means of the porous-plate cell (Fig. 3(b)) for solutions containing 80, 100 and 200 mM Tween 20. The circles on the horizontal axis show the values of H_f corresponding to the steps measured by means of the capillary cell (Fig. 3(a)). In particular, the circles in Fig. 8(c) correspond to the steps in Fig. 7. In this special case, by means of the Scheludko capillary cell we observe eight states with different uniform thickness, whereas with the Mysels–Jones porous-plate cell we detect only four such states (Fig. 8(c)). As mentioned above, the reason for this difference is the low driving pressure applied in the Scheludko–Exerowa capillary cell,^{53,54} which enables one to detect stepwise transitions for thicker films. In contrast, the porous-plate cell of Mysels–Jones⁵⁵ is designed for experiments at higher pressure differences. With the decrease of the concentration of Tween 20, only two metastable states of the film are detected: with zero and one layer of micelles (Fig. 8(a)). The theoretical curves in Fig. 8 are drawn by means of the procedure from Section 4.2.

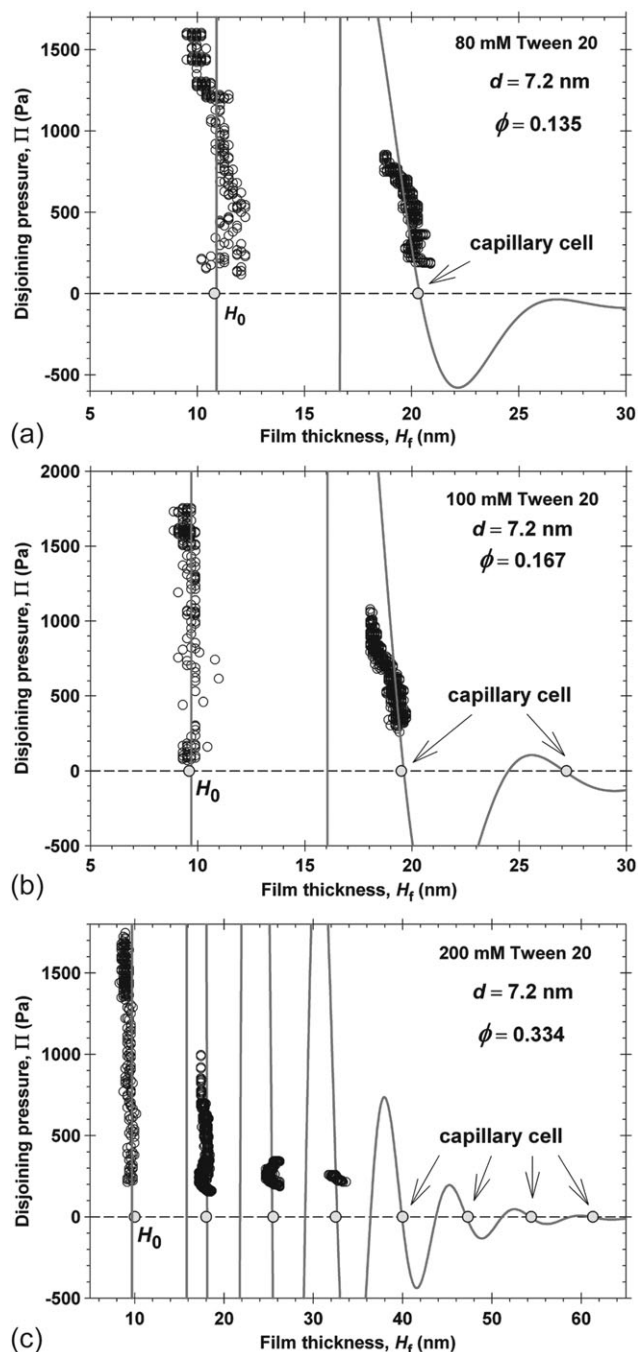


Fig. 8 Disjoining pressure, Π , vs. film thickness, H_f , measured by the porous-plate cell (Fig. 3(b)). (a) 80 mM Tween 20; (b) 100 mM Tween 20; (c) 200 mM Tween 20. The points on the horizontal axis denote the respective values of H_f for the steps measured by the capillary cell (Fig. 3(a)). The solid line shows the best fit of the $\Pi(H_f)$ dependence by means of eqn (7), which corresponds to micelle diameter, d , and volume fraction, ϕ , denoted in the figure.

4 Theoretical background

4.1 Basic equations

Here, we consider spherical Brownian particles, which are confined between the surfaces of a plane-parallel film. The particles will be modelled as hard spheres, and the films

surfaces—as hard walls. The distance between the walls, which is the film thickness, will be denoted by H . The film is in contact (and in chemical equilibrium) with a bulk phase that contains particles of volume fraction ϕ . As mentioned above, each of the two film surfaces induces ordering of the adjacent particles. The degree of ordering decreases with the distance from the wall. The overlap of the structured zones near the two film surfaces gives rise to an excess osmotic pressure in a film of finite thickness H with respect to the bulk osmotic pressure (for $H \rightarrow \infty$). This excess pressure is usually called oscillatory-structural component of disjoining pressure of the film, and is denoted by $\Pi_{\text{osc}}(H)$. Because of the particle ordering, the function $\Pi_{\text{osc}}(H)$ exhibits oscillations, described by a cosine, and since the degree of ordering decreases with the distance from the film surfaces, these oscillations decay with the increase of H ; see ref. 2. Thus, $\Pi_{\text{osc}}(H)$, can be semiempirically described as a product of a cosine with a decaying exponential function:⁴⁴

$$\Pi_{\text{osc}} = P_{\text{hs}} \cos\left(\frac{2\pi H}{d_1}\right) \exp\left(\frac{d^3}{d_1^2 d_2} - \frac{H}{d_2}\right), \text{ for } H > d \quad (2)$$

$$\Pi_{\text{osc}} = -P_{\text{hs}}, \text{ for } 0 < H < d$$

In the case of foam or emulsion films stabilized by surfactant adsorption monolayers, H is the thickness of the water layer sandwiched between the two film surfaces; the total film thickness is $H_f = H + H_0$, where H_0 is the summary thickness of the two adsorption monolayers; see Fig. 6(C); d is the diameter of the hard spheres; d_1 and d_2 are the period and the decay-length of the decaying oscillations; P_{hs} is the (osmotic) pressure of a hard-sphere fluid given by the Carnahan–Starling formula:⁶²

$$\tilde{P}_{\text{hs}} \equiv \frac{P_{\text{hs}} d^3}{kT} = \frac{6}{\pi} \phi \frac{1 + \phi + \phi^2 - \phi^3}{(1 - \phi)^3} \quad (3)$$

where k is the Boltzmann constant; T is the temperature, and \tilde{P}_{hs} is the dimensionless pressure. In eqn (2), d_1 and d_2 are simple functions of the particle volume fraction, ϕ :

$$\frac{d_1}{d} = \sqrt{\frac{2}{3}} + 0.237\Delta\phi + 0.633(\Delta\phi)^2; \frac{d_2}{d} = \frac{0.4866}{\Delta\phi} - 0.42 \quad (4)$$

where $\Delta\phi = 0.7405 - \phi$. The comparison with available numerical data showed that eqn (2) is accurate everywhere except in the region of the first (the highest) oscillatory maximum.

A semiempirical expression for $\Pi_{\text{osc}}(H)$, which is accurate in the whole region $0 \leq H < \infty$, including the region of the first maximum, was proposed by Trokhymchuk *et al.*,⁴⁵ who utilized two additional accurate equations of statistical theory of hard-sphere liquids: the Carnahan–Starling⁶² relation for the chemical potential, $\Delta\mu_{\text{hs}}$:

$$\Delta\tilde{\mu}_{\text{hs}} \equiv \frac{\Delta\mu_{\text{hs}}}{kT} = \phi \frac{8 - 9\phi + 3\phi^2}{(1 - \phi)^3} \quad (5)$$

and the scaled particle theory⁶³ expression for the excess surface free energy of a hard-sphere fluid σ_{hs} :

$$\tilde{\sigma}_{\text{hs}} \equiv \frac{\sigma_{\text{hs}} d^2}{kT} = -\frac{9}{2\pi} \phi^2 \frac{1 + \phi}{(1 - \phi)^3} \quad (6)$$

In eqn (5) and (6), $\Delta\tilde{\mu}_{\text{hs}}$ and $\tilde{\sigma}_{\text{hs}}$ are, respectively, the dimensionless chemical potential and excess surface free energy. Eqn (6) is obtained by substitution of eqn (3) into eqn (1.12) of ref. 63. With the help of the above equations, the following expression for the oscillatory disjoining pressure was obtained:⁴⁵

$$\Pi_{\text{osc}} = -P_{\text{hs}}, \text{ for } 0 \leq h < 1 \quad (7a)$$

$$\frac{\Pi_{\text{osc}} d^3}{kT} = \pi_0 \cos(\omega h + \varphi_2) e^{-qh} + \pi_1 e^{(1-h)\delta}, \text{ for } h \geq 1 \quad (7b)$$

where $h = H/d$ is the dimensionless film thickness; π_0 , π_1 , ω , φ_2 , δ and φ are universal functions of particle volume fraction, ϕ , tabulated in ref. 45; see also Appendix A. By definition, the contribution of the oscillatory structural forces to the interaction energy per unit film area is:

$$W_{\text{osc}}(H) = \int_H^\infty \Pi_{\text{osc}}(\hat{H}) d\hat{H} \quad (8)$$

In other words, $W_{\text{osc}}(H)$ is equal to the work (per unit area) carried out by the oscillatory forces to bring the two film surfaces from infinite separation to a finite distance H . The following accurate semiempirical expression for W_{osc} was obtained:⁴⁵

$$\frac{W_{\text{osc}} d^2}{kT} = -\tilde{P}_{\text{hs}}(1 - h) - 2\tilde{\sigma}_{\text{hs}}, \text{ for } 0 \leq h < 1 \quad (9a)$$

$$\frac{W_{\text{osc}} d^2}{kT} = w_0 \cos(\omega h + \varphi_1) e^{-qh} + w_1 e^{(1-h)\delta}, \text{ for } h \geq 1 \quad (9b)$$

where w_0 , w_1 , and φ_1 are universal functions of ϕ tabulated in ref. 45; see also Appendix A.

In our experiments (Section 3), we investigated nonionic-surfactant systems for which the van der Waals and oscillatory structural surface forces are predominant. In such a case, the contact angle α of the thinnest equilibrium film (of thickness H_0 ; see Fig. 5 and 8) that is sterically stabilized and does not contain micelles (Fig. 6(C)), is given by the expression:⁶⁴

$$\cos\alpha = 1 + \frac{W_{\text{vw}}(0) + W_{\text{osc}}(0, \phi)}{2\sigma} \quad (10)$$

where, as usual, σ is the solution's surface tension. The energy of van der Waals interaction per unit area of this film is²

$$W_{\text{vw}}(0) = -\frac{A_H}{12\pi H_0^2} \quad (11)$$

where A_H is the Hamaker constant. In addition, from eqn (3), (6) and (9a) we obtain:

$$W_{\text{osc}}(0, \phi) = -\frac{6kT}{\pi d^2} \frac{\phi}{(1 - \phi)^3} \left(1 - \frac{\phi}{2} - \frac{\phi^2}{2} - \phi^3\right) \quad (12)$$

Eqn (10)–(12) indicate that the contact angle α is sensitive to the particle volume fraction, ϕ , in the bulk of solution. In the

case of micelles, ϕ is related to the micelle aggregation number:

$$N_{\text{agg}} = \frac{\pi d^3 C_s - \text{CMC}}{6\phi} \quad (13)$$

where C_s is the total surfactant concentration. The total disjoining pressure, Π , is a sum of oscillatory and van der Waals contributions:

$$\Pi = \Pi_{\text{osc}}(H) - \frac{A_H}{6\pi H_f^3} \quad (14)$$

where $H = H_f - H_0$, and $\Pi_{\text{osc}}(H)$ is given by eqn (7). The last term in eqn (14) expresses the van der Waals component of disjoining pressure, Π_{vw} .

4.2 Procedure for data processing

To process simultaneously the experimental data for the contact angles and disjoining pressure, we used the following iteration procedure:

First, we choose a tentative value of the micelle diameter, d . For example, the height of the step in Fig. 7, or the distance between the stable branches of $\Pi(H)$ in Fig. 5 or 8 could serve as a first approximation for d .

Second, for every surfactant concentration, C_s , from the experimental value of the contact angle, α , we determine the micelle volume fraction, ϕ , with the help of eqn (10)–(12). Then, N_{agg} is calculated from eqn (13).

Third, with the latter value of ϕ we fit the data for $\Pi(H_f)$, like those in Fig. 5 and 8, by means of eqn (14); for H_0 we used the experimental thickness of the thinnest stable film that does not contain micelles; d is treated as a single adjustable parameter, whose value is determined from the best fit. Because the diameter, d , of a spherical micelle is not expected to be sensitive to the surfactant concentration (geometrically, d is the summary length of two surfactant molecules, Fig. 6), the $\Pi(H_f)$ data for all C_s are fitted simultaneously, and a single value of d is determined from the fit.

Fourth, with the new value of d , we repeat the calculations starting from the second step above. The procedure is fast convergent and gives d , $\phi(C_s)$ and $N_{\text{agg}}(C_s)$.

5 Numerical results and discussion

5.1 Results for Brij 35

Experimental disjoining pressure isotherms for Brij 35 are shown in Fig. 5. The experimental values of the final film thickness, H_0 , and of the interferometrically measured contact angle, α , are given in Table 1, where the values of α correspond to $H_f = H_0$. As already mentioned, our experimental results for foam films formed from micellar solutions of Brij 35 containing 0 and 100 mM NaCl were practically coinciding. For this reason, in Table 1 we give the mean arithmetic values of H_0 and α measured in these two sets of experiments. In addition, Fig. 5 shows the theoretical $\Pi(H_f)$ curves, which are calculated by means of eqn (14) for $d = 8.8$ nm and the values of ϕ in Table 1. The theoretical curves agree well with the experimental data.

Table 1 Data for Brij 35: experimental film thickness, H_0 , and contact angle, α , and the calculated micelle bulk volume fraction, ϕ , and aggregation number, N_{agg} , corresponding to micelle diameter $d = 8.8$ nm

C_s/mM	H_0/nm	$\alpha/^\circ$	ϕ	N_{agg}
10	14	0.87	0.033	65
50	13	1.64	0.163	66
80	12.5	2.24	0.257	67
100	12	2.65	0.315	69

The values of ϕ and N_{agg} in Table 1 are determined by means of the computational procedure in Section 4.2. The iteration procedure was fast convergent and gave $d = 8.8$ nm. The same value was measured by Phillies *et al.*⁶⁵ by means of dynamic light scattering. The obtained values of N_{agg} (Table 1) slightly increase (from 65 to 69) with the rise of C_s . For comparison, N_{agg} varying between 30 and 65 depending on temperature was obtained by light-scattering methods.⁶⁵ Similar values, $N_{\text{agg}} = 34$ –64 depending on temperature and surfactant concentration, were determined on the basis of SANS measurements.⁶⁶ Latter, the interpretation of the SANS experiments was re-evaluated by means of a reverse Monte Carlo-type method and $N_{\text{agg}} = 60$ –105 was obtained.⁶⁷

In comparison with the other methods, the procedure for determination of N_{agg} from the contact angle α is based on a relatively simple and physically transparent theoretical interpretation, see eqn (10)–(13). In principle, this procedure is applicable also to lower micelle concentrations, at which stratification of the liquid films is not observed, but the contact angle could be measured. An example is the determination of N_{agg} for 10 mM Brij 35 (Table 1), for which stratification is not observed. For this concentration, N_{agg} is calculated from the measured α using the value of d determined from the film-stratification experiments at higher surfactant concentrations. Alternatively, d can be determined by dynamic light scattering.

The obtained values, $N_{\text{agg}} = 65$ –69 (Table 1), are physically reasonable. This can be confirmed by geometrical, molecular-size considerations. For this goal, let us first consider a planar dense adsorption monolayer of Brij 35. From the slope of the surface tension isotherm (at concentrations just below the CMC) we obtained that the area per surfactant molecule is $a_1 = 1.14$ nm². The latter value is close to $a_1 = 1.19$ nm² calculated from the empirical equation⁶⁸ $a_1 = 0.248n^{1/2}$, with $n = 23$ being the number of ethylene-oxide groups in a Brij 35 molecule. Furthermore, the length per ethylene-oxide group is 0.18–0.19 nm in a meander-type polyethylene oxide (PEO) chain.⁶⁹ Hence, for Brij 35 ($n = 23$) the length of the PEO chain is $l_{\text{PEO}} = 4.14$ –4.37 nm in the case of meander-type structure. The latter value agrees well with $l_{\text{PEO}} = H_0/2 - l_{12} = 4.3$ nm, which is calculated by using the experimental $H_0 \approx 12$ nm (Fig. 5) and the length of the C₁₂ paraffin chain of Brij 35 calculated by means of the Tanford^{70,71} formula, $l_{12} = 0.154 + (0.1265 \times 12) = 1.67$ nm. The latter agreement indicates that the PEO chain in the adsorption monolayer of Brij 35 really has a meander structure. (For zigzag structure, l_{PEO} should be about two times greater.) Thus, the volume occupied by the PEO chain of a Brij 35 molecule is estimated to be $v_1 = a_1 l_{\text{PEO}} = 4.93$ –5.20 nm³.

Table 2 Data for Tween 20: experimental film thickness, H_0 , and contact angle, α , and the calculated micelle bulk volume fraction, ϕ , and aggregation number, N_{agg} , corresponding to micelle diameter $d = 7.2$ nm

C_s/mM	H_0/nm	$\alpha/^\circ$	ϕ	N_{agg} (eqn (13))
80	10.4	1.87 ± 0.04	0.135	70
100	10.2	2.09 ± 0.03	0.167	70
200	10.1	3.45^a	0.334	70

^a Calculated as explained in the text.

Next, the total volume occupied by the PEO chains in a spherical micelle of Brij 35 is $V_{\text{PEO}} = (4/3)\pi(R_m^3 - l_{12}^3) = 337.3 \text{ nm}^3$, where we have substituted $R_m \equiv d/2 = 4.4 \text{ nm}$ and $l_{12} = 1.67 \text{ nm}$. Finally, $N_{\text{agg}} = V_{\text{PEO}}/v_1 = 65\text{--}68$, which agrees very well with the values of N_{agg} in Table 1, which have been independently determined from the measured contact angle.

5.2 Results for Tween 20

Table 2 shows the experimental film thickness, H_0 , for the final state with zero layers of micelles, and the contact angle, α , in this state. We succeeded to measure α only for $C_s = 80$ and 100 mM Tween 20. For 200 mM Tween 20 the interference rings at the film periphery were too dense due to the larger meniscus slope, which makes the interferometric determination of α rather inaccurate. The values in the last two columns of Table 2 are determined by means of the procedure for data interpretation described in Section 4.2.

From the average high of the steps in Fig. 7, we obtained a first approximation for the micelle diameter, $d \approx 7.2 \text{ nm}$. With the latter value of d , from the experimental values of the contact angle α in Table 2 we calculated $N_{\text{agg}} = 70$ for both $C_s = 80$ and 100 mM Tween 20, using eqn (10)–(13). The respective calculated micelle volume fractions are $\phi = 0.135$ and 0.167 . Assuming that $d = 7.2$ and $N_{\text{agg}} = 70$ also for $C_s = 200 \text{ mM}$, and using eqn (13), we calculated $\phi = 0.334$ for the latter concentration, for which the contact angle could not be measured. Substituting $\phi = 0.334$ in eqn (10)–(12), we estimate $\alpha = 3.45^\circ$ for $C_s = 200 \text{ mM}$. With the obtained parameter values, we plotted the theoretical oscillatory curves shown in Fig. 8. As seen in the latter figure, the agreement between theory and experiment is very good. For this reason, further variations (adjustment) of the value of d were not necessary.

6 Effect of the oscillatory structural forces on the stability of dispersions

6.1 Energy of interaction between two large colloid spheres immersed in a fluid of small colloid spheres

The agreement between theory and experiment established in Section 5 represents additional evidence in favour of the correctness of the used theoretical expressions, which have been also successfully tested against numerical data from Monte Carlo simulations.⁴⁵ As a next step, here we apply the theoretical approach by Trokhymchuk *et al.*⁴⁵ to investigate the effect of the oscillatory structural forces on the stability of dispersions. Our attention will be focused on the

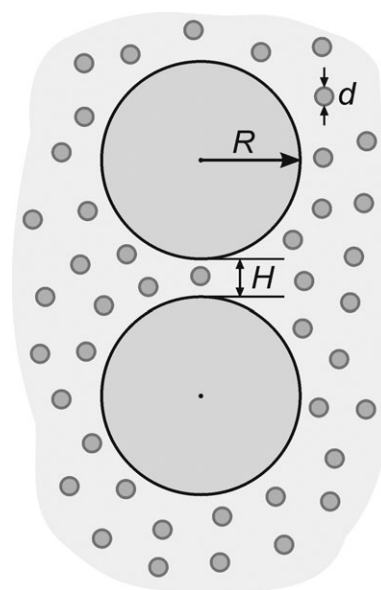


Fig. 9 Sketch of two large colloidal spheres of radius R , which are immersed in a fluid of small hard spheres, of diameter, d .

interplay of the van der Waals and oscillatory forces and on the possible stability–instability transitions.

First we will calculate the energy of interaction between two large colloidal spheres of radius R , which are immersed in a fluid of smaller colloidal spheres of diameter d (Fig. 9). We will use the Derjaguin approximation:⁷²

$$U(H, \phi) = \pi R \int_H^\infty W(\hat{H}, \phi) d\hat{H} \quad (15)$$

Here, $U(H)$ is the energy of interaction between the two spherical particles (of radius R) separated at a surface-to-surface distance H (Fig. 9), whereas $W(\hat{H})$ is the interaction energy per unit area of a plane-parallel film of thickness \hat{H} . Substituting $W = W_{\text{osc}}$ in eqn (15), with the help of eqn (9) we derive:

$$U_{\text{osc}}(H, \phi) = kT \frac{R}{d} u_{\text{osc}}(h, \phi) \quad (h = H/d) \quad (16)$$

where $u_{\text{osc}}(h, \phi)$ is an universal dimensionless function of h and ϕ defined as follows:

$$u_{\text{osc}}(h, \phi) = \frac{\pi W_0}{\omega^2 + q^2} [q \cos(\omega h + \varphi_1) - \omega \sin(\omega h + \varphi_1)] e^{-qh} + \frac{\pi W_1}{\delta} e^{(1-h)\delta}, \quad \text{for } h \geq 1 \quad (17a)$$

$$u_{\text{osc}}(h, \phi) = -\frac{\pi}{2} [(1-h)\tilde{P}_{\text{hs}} + 4\tilde{\sigma}_{\text{hs}}](1-h) + u_{\text{osc}}(1, \phi), \quad \text{for } 0 \leq h \leq 1 \quad (17b)$$

Here, \tilde{P}_{hs} and $\tilde{\sigma}_{\text{hs}}$ are defined by eqn (3) and (6), and $u_{\text{osc}}(1, \phi)$ is given by eqn (17a) for $h = 1$; see also Appendix A.

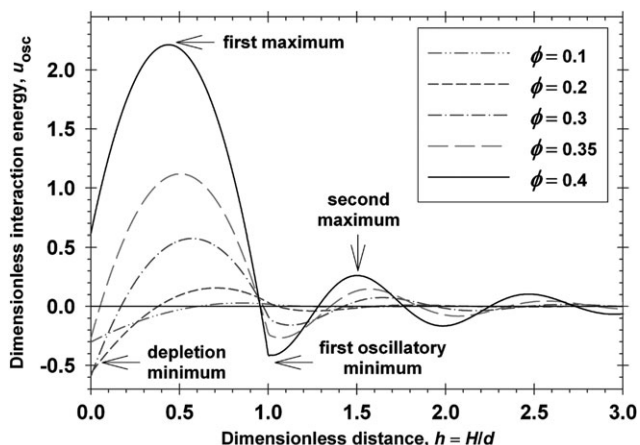


Fig. 10 Plot of the dimensionless energy of interaction, u_{osc} , vs. the dimensionless surface-to-surface distance, h , between two large colloidal spheres. The $u_{\text{osc}}(h)$ curves are calculated by means of eqn (17) for several different volume fractions, ϕ , of the small particles; see Fig. 9.

Fig. 10 shows plots of u_{osc} vs. h calculated by means of eqn (17) for several different volume fractions, ϕ , of the small particles. As expected, the amplitude of the oscillations markedly increases with the rise of ϕ , the first maximum always having the greatest amplitude. Because the dimensional energy is $U_{\text{osc}} \propto (R/d)u_{\text{osc}}$, the amplitude of the oscillations could be much greater than the thermal energy kT . For example, if the large particles are emulsion drops of radius 8 μm and the small particles are surfactant micelles of diameter 8 nm, then the scaling factor will be $R/d = 1000$. The minima of the oscillatory curves in Fig. 10 correspond to stable equilibrium states of the doublet of two large particles, whereas the maxima represent energy barriers separating the stable states.

For the lower ϕ , the depletion minimum, $u_{\text{osc}}(0, \phi)$, is the deepest one. At $\phi = 0.26$, its depth is maximal: $u_{\text{osc}}(0, 0.26) = -0.64$. For $\phi > 0.26$, $u_{\text{osc}}(0, \phi)$ increases, and for $\phi > 0.37$ it becomes positive. Nevertheless, the depletion minimum always corresponds to particle aggregation because the first oscillatory maximum serves as a high barrier to particle detachment.

This behaviour of $u_{\text{osc}}(0, \phi)$ calls for some discussion. In view of the general relation, eqn (15), the energy of oscillatory-structural interaction between two particles, $U_{\text{osc}}(H, \phi)$, is an integral of the respective interaction energy for a plane-parallel film, $W_{\text{osc}}(H, \phi)$. At close contact between the two surfaces (for a very thin film without micelles), the depth of the depletion minimum, $|W_{\text{osc}}(0, \phi)|$, is an increasing function of ϕ ; see eqn (12). Physically, this means that the depletion attraction (due to the sucking osmotic pressure engendered by the micelles in the bulk phase) increases with the rise of ϕ . Because $U_{\text{osc}}(0, \phi)$ is an integral of $W_{\text{osc}}(H, \phi)$, it contains contributions from $W_{\text{osc}}(H, \phi)$ for every $H > 0$, including zones of negative and positive W_{osc} . Physically, this is related to the fact that the gap between two spherical particles (Fig. 9) has a non-uniform thickness, where the local excess pressure could be attractive or repulsive depending on the local thickness. For this reason, it is not obvious whether the attraction or repulsion will prevail in the integral interaction energy between two spherical particles in contact, $U_{\text{osc}}(0, \phi)$. Fig. 10 shows that both cases are possible depending on the value of ϕ . In particular, substituting $h = 0$ in

eqn (17b), one obtains a relatively simple expression for calculating the depth of the depletion minimum:

$$u_{\text{osc}}(0, \phi) = -\frac{\pi}{2}(\tilde{P}_{\text{hs}} + 4\tilde{\sigma}_{\text{hs}}) + u_{\text{osc}}(1, \phi) \quad (18)$$

The calculations of $u_{\text{osc}}(h, \phi)$ indicate that the first (the highest) maximum is located in the interval $0 < h < 1$. For this reason, its position, $h_{1,\text{max}}$, and height can be calculated by differentiation of eqn (17b):

$$h_{1,\text{max}} = 1 + \frac{2\tilde{\sigma}_{\text{hs}}}{\tilde{P}_{\text{hs}}} = 1 - \frac{\phi(1+\phi)}{1+\phi+\phi^2-\phi^3} \quad (19)$$

$$u_{\text{osc}}(h_{1,\text{max}}, \phi) = 2\pi \frac{\tilde{\sigma}_{\text{hs}}^2}{\tilde{P}_{\text{hs}}} + u_{\text{osc}}(1, \phi) \quad (20)$$

The dependencies of the position and height of the first oscillatory maximum on ϕ is illustrated in Fig. 11(a). The exponential increase of $u_{\text{osc}}(h_{1,\text{max}}, \phi)$ with the rise of ϕ comes from the exponential functions in $u_{\text{osc}}(1, \phi)$, see eqn (17a). From eqn (17a) we calculated also the position of the first oscillatory minimum, $h_{1,\text{min}}$, and its depth, $u_{\text{osc}}(h_{1,\text{min}}, \phi)$, as well as the position of the second oscillatory maximum, $h_{2,\text{max}}$, and its height, $u_{\text{osc}}(h_{2,\text{max}}, \phi)$; see Fig. 11(b) and (c). Because the scaling factor R/d in eqn (16) can be of the order of 1000, the two particles could flocculate also in the first oscillatory minimum.

Next, we consider the interplay of the oscillatory structural and van der Waals surface forces. The van der Waals interaction energy per unit area of a plane-parallel film is:² $W_{\text{vw}} = -A_{\text{H}}/[12\pi(H_0 + H)^2]$. The substitution of the latter equation in eqn (15) yields the respective energy of interaction between two spherical particles of radius R :

$$U_{\text{vw}}(H) = kT \frac{R}{d} u_{\text{vw}}(h); \quad u_{\text{vw}}(h) \equiv -\frac{A_{\text{H}}}{12kT(h_0 + h)} \quad (21)$$

where $h_0 \equiv H_0/d$, and $u_{\text{vw}}(h)$ is the dimensionless van der Waals interaction energy. In view of eqn (16) and (21), the total energy of interaction between the two large particles (Fig. 9) is:

$$U(H, \phi) = kT \frac{R}{d} u(h, \phi) \quad (22)$$

$$u(h, \phi) = u_{\text{osc}}(h, \phi) + u_{\text{vw}}(h) \quad (23)$$

where $u_{\text{osc}}(h, \phi)$ and $u_{\text{vw}}(h)$ are given by eqn (17) and (21), and $u(h, \phi)$ is the total dimensionless interaction energy, which is a universal function that is independent on R and d , but depends on the Hamaker constant, A_{H} , through eqn (21).

In Fig. 12(a), we have plotted u vs. h for three different values of ϕ , and for typical values of the other parameters: $h_0 = 1$; $T = 25^\circ\text{C}$, and $A_{\text{H}} = 4 \times 10^{-21}$ J. The latter value of A_{H} corresponds to emulsion systems, for which the two large particles in Fig. 9 represent emulsion drops. For $\phi = 0.3$, the first and the second maxima are high enough and serve as barriers to particle (drop) flocculation. For $\phi = 0.2$, only the first maximum is high enough and could prevent flocculation. For $\phi = 0.1$, u is negative at the first maximum, and it cannot prevent flocculation of the two particles (drops).

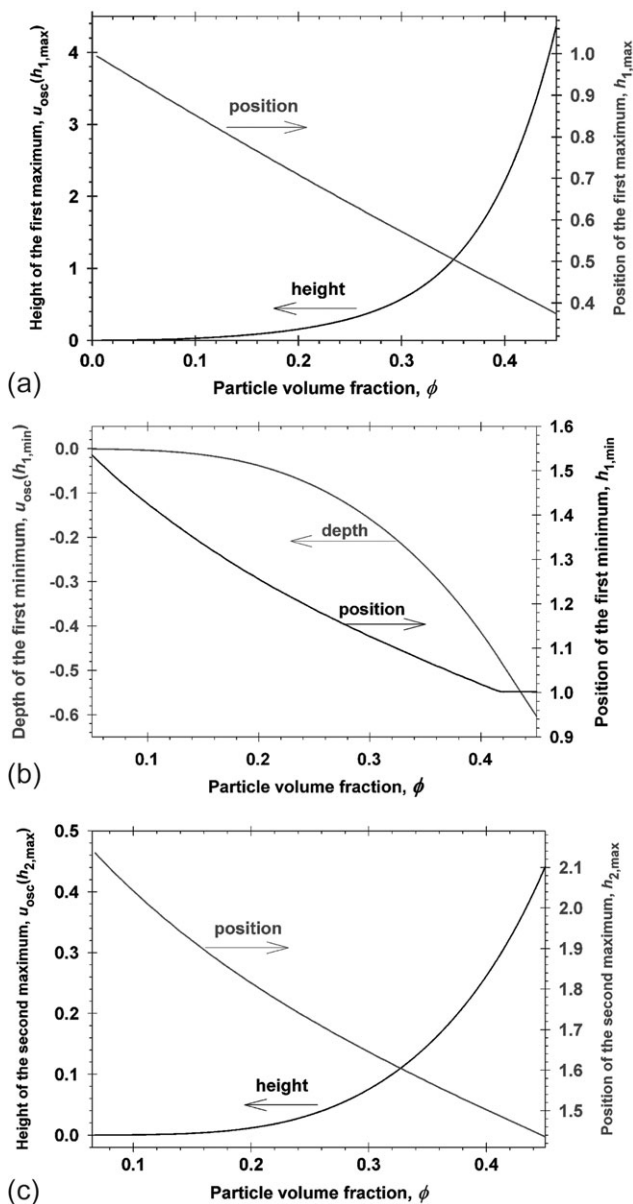


Fig. 11 Dependence of the height (depth) of the oscillatory maxima (minima) and their position on the volume fraction of the small particles, ϕ . (a) Height and position of the first maximum. (b) Depth and position of the first minimum. (c) Height and position of the second maximum.

Fig. 12(b) shows a similar plot of u vs. h , with the only difference that this time the Hamaker constant is $A_H = 4 \times 10^{-20}$ J. The latter value of A_H is typical for foam systems, for which the two large particles in Fig. 9 represent gas bubbles. (Similar, and even higher, values of A_H can be realized with solid particles dispersed in a liquid phase.) This time, only for $\phi = 0.3$, the first maximum is high enough and serves as a barrier to particle (bubble) flocculation (or coalescence). In contrast, for $\phi = 0.1$ and 0.2 , u is negative for all values of h , which means that the contribution from the oscillatory structural force cannot prevent the flocculation of the two particles.

The numerical results in Fig. 12 indicate that the van der Waals attraction could be strong enough to overcome the

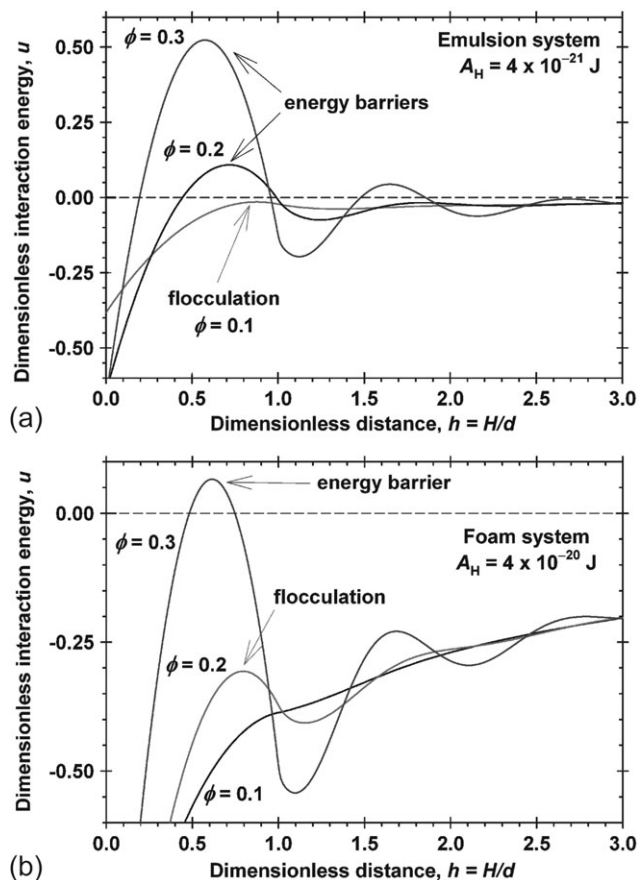


Fig. 12 Plot of the total dimensionless interaction energy, $u = u_{osc} + u_{vw}$, vs. h for three different values of ϕ , and for typical values of the other parameters: $h_0 = 1$; $T = 25^\circ\text{C}$. (a) Emulsion system with $A_H = 4 \times 10^{-21}$ J. (b) Foam system with $A_H = 4 \times 10^{-20}$ J. With the decrease of the particle volume fraction, ϕ , the height of the highest maximum, $u(h_{1,max})$, decreases; flocculation occurs at $u(h_{1,max}) \leq 0$.

stabilizing effect of the oscillatory structural force and to cause flocculation in the depletion minimum. Thanks to the van der Waals attraction, the depletion minimum becomes always deeper than the first oscillatory minimum, which is not always the case if van der Waals forces were missing; compare Fig. 10 and 12.

6.2 DLVO-type criterion for coagulation

The dispersion can be protected from flocculation if the volume fraction of the small particles is increased above a certain critical value, ϕ_{cr} . To determine ϕ_{cr} , we can apply a criterion analogous to that used in the DLVO theory:

$$U(h_{cr}, \phi_{cr}) = 0 \quad (24)$$

$$\frac{\partial U}{\partial h}(h_{cr}, \phi_{cr}) = 0 \quad (25)$$

Eqn (24) means that the onset of coagulation corresponds to $U = 0$ at the top of the barrier; eqn (25) reflects the fact that the barrier corresponds to a local maximum of U . The substitution of U from eqn (22) into eqn (24) and (25) leads to a system of two equations for determining h_{cr} and ϕ_{cr} . We

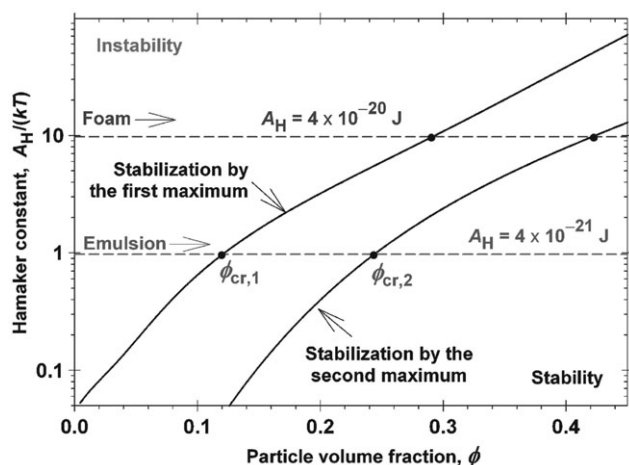


Fig. 13 Stability–instability diagram in the plane (ϕ, A_H) . The two solid lines represent the dependence $\phi_{cr}(A_H)$ calculated for the first and the second maximum. The lower and upper horizontal dashed lines correspond, respectively, to emulsion and foam systems of Hamaker constants $A_H = 4 \times 10^{-21}$ J and $A_H = 4 \times 10^{-20}$ J. The intersection points of these horizontal lines with the two solid lines give the critical volume fractions for stabilization of the respective dispersions by the first and second maximum.

solved this system numerically for different values of the Hamaker constant, A_H , and obtained $\phi_{cr}(A_H)$; the other parameter values are $h_0 = 1$, and $T = 25$ °C.

The results are shown in Fig. 13 in the form of a stability–instability diagram in the plane (ϕ, A_H) . The two curves represent the dependence $\phi_{cr}(A_H)$ calculated for the first and the second maximum. The lower horizontal dashed line corresponds to an *emulsion* system of Hamaker constant $A_H = 4 \times 10^{-21}$ J. The intersection points of this horizontal line with the two solid lines give the critical volume fractions of the small particles as follows: $\phi_{cr,1} = 0.12$ for stabilization by the first maximum, and $\phi_{cr,2} = 0.24$ for stabilization by the second maximum. In other words, For $0 < \phi < 0.12$ the drops will flocculate; for $0.12 < \phi < 0.24$ the drops will be stabilized by the first maximum; for $\phi > 0.24$ the second maximum becomes high enough to serve as an additional barrier to flocculation.

In Fig. 13, the upper horizontal dashed line corresponds to a *foam* system of Hamaker constant $A_H = 4 \times 10^{-20}$ J. In this case, the van der Waals attraction is stronger and the oscillatory structural forces are able to stabilize the system at higher volume fractions of the small particles: $\phi_{cr,1} = 0.29$ for stabilization by the first maximum, and $\phi_{cr,2} = 0.42$ for stabilization by the second maximum. In other words, For $0 < \phi < 0.29$ the bubbles will flocculate; for $0.29 < \phi < 0.42$ the bubbles will be stabilized by the first maximum; for $\phi > 0.42$ the second maximum becomes high enough to serve as a second barrier to flocculation.

A more precise formulation of the flocculation criterion could be given, in which, eqn (24) is exchanged by

$$U(h_{cr}, \phi_{cr}) = kT \quad (26)$$

In other words, to prevent the flocculation (coagulation) the height of the barrier should be greater than kT , instead of

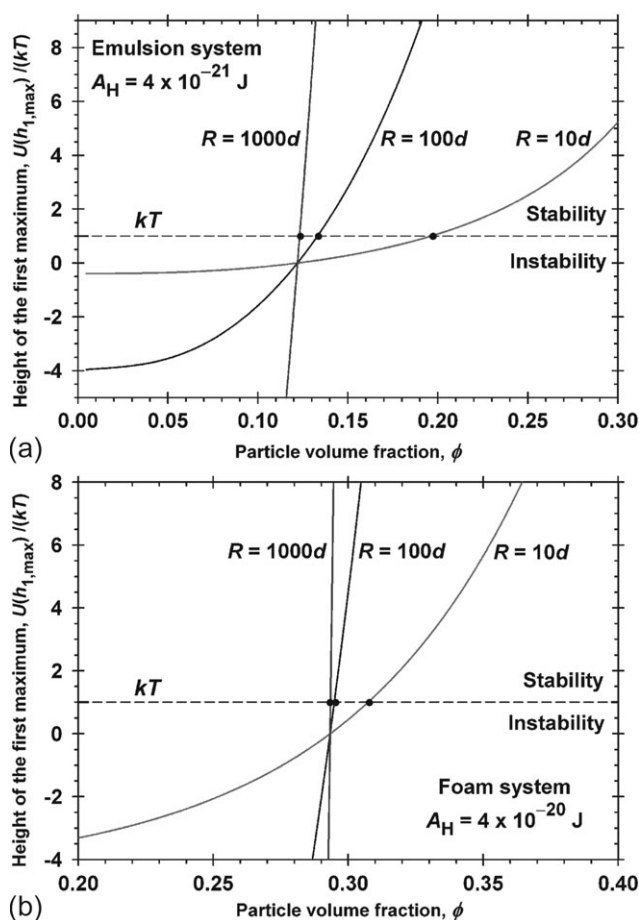


Fig. 14 The height of the first maximum of the total interaction energy, $U = U_{osc} + U_{vw}$, plotted vs. the volume fraction of the small particles, ϕ . The dispersion of the large colloidal particles will be stable for $U > kT$, and unstable—for $U < kT$. (a) Emulsion system with $A_H = 4 \times 10^{-21}$ J. (b) Foam system with $A_H = 4 \times 10^{-20}$ J.

greater than zero. In view of eqn (16), the criterion (26) acquires the form:

$$u(h_{cr}, \phi_{cr}) = \frac{d}{R} \quad (27)$$

For $d/R \ll 1$, eqn (27) reduces to eqn (24). If the ratio d/R is not so small, eqn (27) could lead to some dependence of ϕ_{cr} on R . To illustrate this, in Fig. 14 we have plotted the height of the first barrier, $U(h_{1,max})$, vs. ϕ for different R/d . The intersection points of these plots with the horizontal line $U(h_{1,max}) = kT$ define ϕ_{cr} . The decrease of R/d from 1000 to 10 leads to an increase of ϕ_{cr} from 0.12 to 0.20 for an emulsion system (Fig. 14(a)) and from 0.29 to 0.31 for a foam system (Fig. 14(b)).

6.3 The second virial coefficient

Here, we consider the effect of the oscillatory structural forces on the second virial coefficient of Brownian colloidal spheres of radius R , which are immersed in a fluid that contains smaller particles of diameter d (Fig. 9). The general definition of the second virial coefficient in the expansion of osmotic

pressure, B_2 , is:⁷³

$$B_2 = 4\left(\frac{4}{3}\pi R^3\right) + 2\pi \int_{2R}^{\infty} \left[1 - \exp\left(-\frac{U}{kT}\right)\right] r^2 dr \quad (28)$$

where $r = 2R + H$ is the centre-to-centre distance between the two colloidal spheres. The first term in the right-hand side of eqn (28) accounts for the volume excluded by the two particles of radius R . For computational purposes, it is convenient to represent eqn (28) in the form:

$$B_2 = 4\left(\frac{4}{3}\pi R^3\right)(1 + b_2) \quad (29)$$

where the dimensionless coefficient, b_2 , is defined by the relationship:

$$b_2 \equiv \frac{3d}{2R} \int_0^{\infty} \left[1 - \exp\left(-\frac{U}{kT}\right)\right] \left(1 + \frac{hd}{2R}\right)^2 dh \quad (30)$$

($h = H/d$). Usually, $B_2 > 0$ is considered as an indicator for predominant repulsion, whereas $B_2 < 0$ —for predominant attraction.⁷³ In view of eqn (29), these relations could be reformulated in terms of the dimensionless parameter b_2 :

$$\begin{aligned} b_2 > -1 &: \text{predominant repulsion;} \\ b_2 < -1 &: \text{predominant attraction} \end{aligned} \quad (31)$$

Fig. 15 shows plots of $-b_2$ vs. ϕ calculated by means of eqn (22), (23) and (30), for two values of particle radius, R , and for two values of the Hamaker constant, A_H . As seen in Fig. 15, b_2 is almost everywhere smaller than -1 , which means “predominant attraction” according to eqn (31). This result follows from the fact that the exponential function in eqn (30) cuts the contributions from the oscillatory maxima, but amplifies the contributions from the minima. In fact, the value of the integral in eqn (30) is dominated by the deepest minimum, which is the depletion minimum.

In general, the second virial coefficient B_2 (and b_2) is a thermodynamic quantity, which takes into account the fact that the small particles may cause flocculation of the large particles in the depletion minimum (or in the oscillatory minima). Thermodynamic equilibrium can be achieved by equilibration of the two opposite processes of particle attachment and detachment. However, from kinetic viewpoint, the two interacting particles could never reach the depletion minimum, because of the high barrier due to the first maximum; see Fig. 10. For this reason, a more adequate characteristic of the stability to flocculation could be the kinetic Fuchs factor.

6.4 The kinetic Fuchs factor

In the theory of slow coagulation (flocculation), the concentration of aggregates, c , obeys the equation:^{47,74–76}

$$\frac{dc}{dt} = -\frac{a}{2}c^2; \quad a = \frac{8\pi D_R R}{W_F} \quad (32)$$

Here, a is a kinetic rate constant; D_R is a relative diffusivity, and W_F is the Fuchs factor, which is dimensionless and is

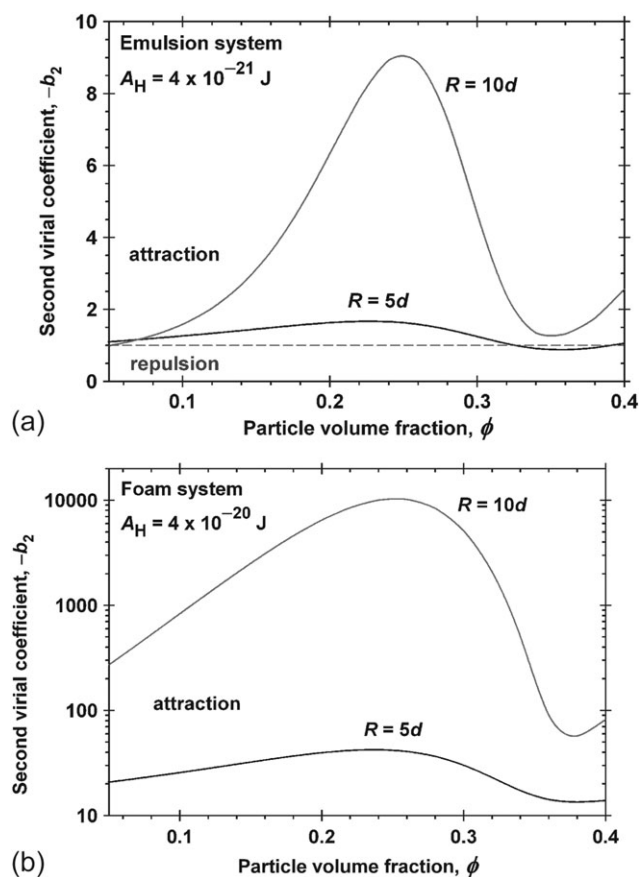


Fig. 15 The dimensionless second virial coefficient, $-b_2$, defined by eqn (30), as a function of the volume fraction of the small particles, ϕ , for two values of the large-particle radius, R . (a) Emulsion system with $A_H = 4 \times 10^{-21}$ J. (b) Foam system with $A_H = 4 \times 10^{-20}$ J.

defined by the integral:^{47,74–76}

$$W_F = 2 \int_0^{\infty} \frac{\beta(s)}{(2+s)^2} \exp\left[\frac{U(s)}{kT}\right] ds \quad (33)$$

where $s = H/R$ is the dimensionless surface-to-surface distance between two particles of radius R ; U is the interaction energy due to surface forces, and $\beta(s)$ accounts for the hydrodynamic interactions. An approximated expression, $\beta(s) \approx 1/2s$, is usually applied,⁷⁵ which follows from the asymptotic Taylor formula⁷⁷ for the hydrodynamic interaction between two spherical particles. Then, eqn (33) acquires the form:

$$W_F = \int_0^{\infty} \frac{1}{(h+h_m)} \left(2 + h\frac{d}{R}\right)^{-2} \exp\left[\frac{U(h)}{kT}\right] dh \quad (34)$$

where h_m is a molecular cut-off parameter (of the order of the diameter of the solvent molecule); W_F is not sensitive to h_m because the value of W_F is determined mostly by the first maximum of $U(h)$. This is due to the fact that the integrand in eqn (34) contains $\exp(+U/kT)$, which amplifies the contribution of the highest maximum, in contrast with the factor $\exp(-U/kT)$ in eqn (30) that amplifies the contribution from the deepest minimum. The physical meaning of W_F follows from eqn (32): For $W_F > 1$, the coagulation is decelerated; for

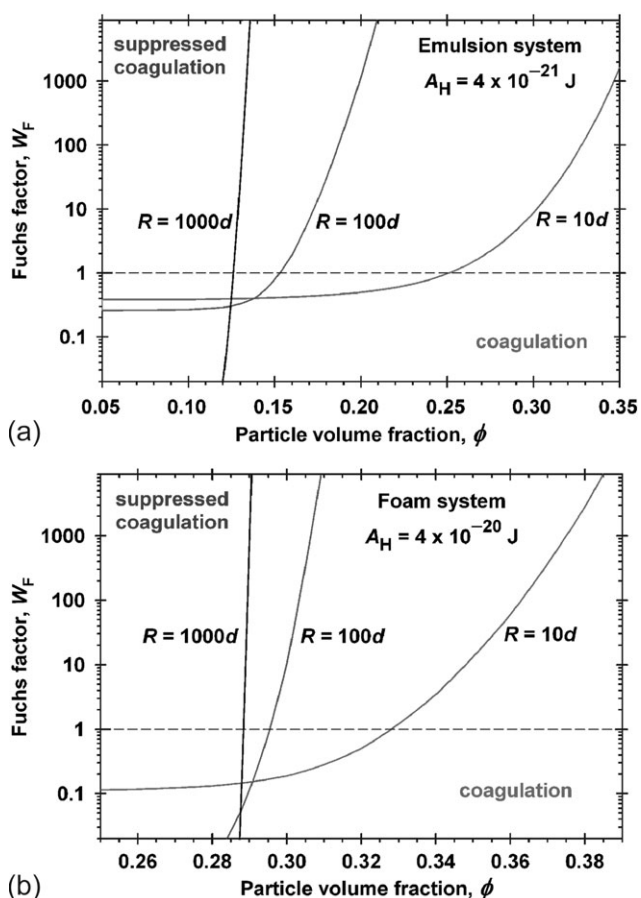


Fig. 16 The Fuchs factor, W_F , defined by eqn (34), plotted vs. the volume fraction of the small particles, ϕ , for three values of the large-particle radius, R , denoted in the figure. For $W_F > 1$, the coagulation is suppressed. (a) Emulsion system with $A_H = 4 \times 10^{-21}$ J. (b) Foam system with $A_H = 4 \times 10^{-20}$ J.

$W_F < 1$, the coagulation is accelerated, whereas for $W_F = 1$ we are dealing with fast coagulation in the Smoluchowski regime.^{47,74–76}

Fig. 16 shows plots of W_F vs. ϕ , which are calculated by means of eqn (34), where $U(h)$ is given by eqn (22) and (23); $R/d = 10, 100$, and 1000 . In terms of the considered criterion, the stability–instability transition is equivalent to a transition from slow to fast coagulation, which happens at $W_F = 1$ (the horizontal dashed line in Fig. 16). By shape, the curves in Fig. 16 resemble those in Fig. 14. This is not occasional, because the curves in Fig. 14 are calculated on the basis of the DLVO-type stability criterion applied to the first maximum, see eqn (25) and (26), and the value of W_F in eqn (34) is determined by the same first maximum of $U(h)$. In other words, the two criteria for stability–instability transition, which are illustrated in Fig. 14 and 16, give similar predictions. In both cases, “instability” means coagulation in the depletion minimum, whereas “stability” means that the barrier due to the first maximum is high enough to prevent such coagulation. However, as mentioned above, this stability does not exclude a weak coagulation in the first oscillatory minimum. The increase of the radius R of the bigger particles at a given ϕ leads to an increasing stability of the dispersion of these particles;

see Fig. 14 and 16. The effect of R is pronounced for smaller particles ($R \approx 10d$), whereas for bigger particles ($R > 100d$) this effect is negligible.

7 Summary and conclusions

This study is devoted to a quantitative comparison of theory and experiment in the field of oscillatory structural forces that are due to the confinement of colloidal particles in a thin liquid film. Our first goal was to determine the aggregation number and diameter of surfactant micelles by measurements with liquid films. Micellar solutions of two nonionic surfactants, Brij 35 and Tween 20, have been used. With the help of a capillary cell (Fig. 3(a)), we recorded the step-wise thinning of the film (Fig. 4 and 7), and determined the contact angles from the interference rings (Tables 1 and 2). Furthermore, by means of a porous-glass cell (Fig. 3(b)), we obtained experimental disjoining-pressure isotherms, $\Pi(h)$; see Fig. 5 and 8. A procedure for theoretical data interpretation was developed (Section 4.2), which is based on the accurate expressions for the oscillatory structural force obtained by Trokhymchuk *et al.*⁴⁵ The nonionic surfactant micelles are modelled as hard spheres. The determined micelle diameter and aggregation number for Brij 35 and Tween 20 agree well with results of other experimental methods and theoretical estimates (Section 5). Thus, it turns out that the measurement of thickness and contact angles of thin liquid films could give information about the micelles, which is similar to that obtainable by dynamic and static light scattering.

Our second goal was to investigate the predictions of different quantitative criteria for stability–instability transitions, having in mind that the oscillatory forces exhibit both maxima, which play the role of barriers to coagulation, and minima that could produce flocculation or coalescence in colloidal dispersions (emulsions, foams, suspensions). Because the present study is restricted to nonionic systems, we investigated the interplay of the oscillatory structural force with the van der Waals surface force (Fig. 12). The two kinetic criteria, *viz.* the DLVO-type criterion (Section 6.2) and the Fuchs criterion (Section 6.4) give similar and physically reasonable predictions about the stability–instability transitions and can be used to construct stability–instability diagrams (Fig. 13–16). These diagrams show the values of the micelle volume fraction, for which the oscillatory barriers prevent the particles from coming into close contact, or for which a strong flocculation in the depletion minimum or a weak flocculation in the first oscillatory minimum could be observed.

Possible future directions could include the extension and application of the above approach to other systems such as mixed micelles, ABA block copolymers, and polyelectrolyte/surfactant systems. In this respect, the greatest challenge is the extension of the approach to ionic micelles and other charged particles, for which computer simulations by means of the canonical Monte Carlo method have been successfully applied,^{42,78} but accurate analytical expressions, like those in Section 4, are still missing. Furthermore, the effect of divalent and multivalent counterions on the structuring of charged particles in liquid films could be investigated. Another broad research field is the effect of the structural forces in the case of

non-spherical particles like rod-like micelles. Dynamic aspects could be also important, such as the motion of the contact line at the periphery of a particle-containing film, in relation to the phenomena wetting and spreading. The maxima and minima of the oscillatory force are expected to give rise to a considerable contact-angle hysteresis, which could be stronger than that in the case of DLVO forces.⁷⁹ An additional broad field is the analysis, modelling, prediction and control of the stability of various dispersions containing bigger and smaller particles (Fig. 9) by extension and application of the methods and criteria considered in Section 6.

Appendix A: Calculation of the oscillatory-structural disjoining pressure and interaction energy

In accordance with the approach developed by Trokhymchuk *et al.*,⁴⁵ the oscillatory-structural component of disjoining pressure and interaction energy, $\Pi_{\text{osc}}(h, \phi)$ and $W_{\text{osc}}(h, \phi)$, are calculated, respectively, by means of eqn (7) and (9), where P_{hs} and σ_{hs} are given by eqn (3) and (6), and the other parameters are:

$$\omega = 4.45160 + 7.10586\phi - 8.30671\phi^2 + 8.29751\phi^3 \quad (\text{A1})$$

$$\varphi_1 = 0.40095 + 2.10336\phi \quad (\text{A2})$$

$$\varphi_2 = -0.39687 - 0.3948\phi + 2.3027\phi^2 \quad (\text{A3})$$

$$q = 4.78366 - 19.64378\phi + 37.37944\phi^2 - 30.59647\phi^3 \quad (\text{A4})$$

$$\pi_0 = 4.06281 - 3.10572\phi + 76.67381\phi^2 \quad (\text{A5})$$

$$w_0 = 0.57909 + 0.83439\phi + 8.65315\phi^2 \quad (\text{A6})$$

$$\pi_1 = \frac{6}{\pi}\phi \exp\left(\frac{\Delta\mu_{\text{hs}}}{kT}\right) - \frac{pd^3}{kT} - \pi_0 \cos(\omega + \varphi_2)\exp(-q) \quad (\text{A7})$$

$$\delta = \frac{\pi_1}{w_1}; \quad w_1 = -\frac{2\sigma_{\text{hs}}d^2}{kT} - w_0 \cos(\omega + \varphi_1)\exp(-q) \quad (\text{A8})$$

In eqn (A7), the quantity $\Delta\mu_{\text{hs}}$ is defined by eqn (5).

List of symbols

A_{H}	Hamaker constant
B_2	second virial coefficient, eqn (28)
b_2	dimensionless second virial coefficient, eqn (30)
CMC	critical micellization concentration
C_s	total surfactant concentration
d	diameter of the small colloid particles (Fig. 9)
d_1	period of the oscillations, eqn (2) and (4)
d_2	decay length of the oscillations, eqn (2) and (4)
H	film thickness or the shortest surface-to-surface distance (Fig. 9)
H_0	thickness of the two surfactant adsorption monolayers

(continued)

$H_{\text{f}} = H + H_0$	total thickness of a foam or emulsion film
$h = H/d$	dimensionless H
$h_0 = H_0/d$	dimensionless H_0
h_{cr}	critical value of h for onset of coagulation
$h_{1,\text{max}}$	value of h for the first oscillatory maximum
$h_{1,\text{min}}$	value of h for the first oscillatory minimum
$h_{2,\text{min}}$	value of h for the second oscillatory maximum
I	intensity of light reflected from the film
k	the Boltzmann constant
N_{agg}	aggregation number of the micelles
n_{f}	refractive index of the liquid forming the film
P_{hs}	osmotic pressure of a hard-sphere fluid; eqn (3)
q	parameter defined by eqn (A4)
R	radius of the bigger particles (Fig. 9)
T	temperature
U	interaction energy between two bigger particles, eqn (15)
U_{osc}	oscillatory component of U
U_{vw}	van der Waals component of U
u	dimensionless U , eqn (22)
u_{osc}	oscillatory component of u , eqn (17)
u_{vw}	van der Waals component of u , eqn (21)
W	excess free energy of the film
W_{osc}	oscillatory component of W , eqn (8)
W_{vw}	van der Waals component of W
W_{F}	Fuchs factor; eqn (33)
w_0	parameter defined by eqn (A6)
w_1	parameter defined by eqn (A8)
α	contact angle of the thinnest equilibrium film, eqn (9)
β	hydrodynamic interaction factor, eqn (33)
$\Delta\mu_{\text{hs}}$	concentration part of the chemical potential of a hard-sphere fluid, eqn (5)
δ	parameter defined by eqn (A8)
λ	wavelength of monochromatic light
Π	disjoining pressure
Π_{osc}	oscillatory component of disjoining pressure
Π_{vw}	van der Waals component of disjoining pressure
π_0	parameter defined by eqn (A5)
π_1	parameter defined by eqn (A7)
σ	surface tension
σ_{hs}	excess surface free energy of a hard-sphere fluid, eqn (6)
ϕ	volume fraction of the small colloid particles
ϕ_{cr}	critical value of ϕ for onset of coagulation
φ_1	parameter defined by eqn (A2)
φ_2	parameter defined by eqn (A3)
ω	parameter defined by eqn (A1)

Acknowledgements

We gratefully acknowledge the support of Unilever Research & Development, Trumbull, Connecticut, for this study. One of

us (P. K.) thanks Prof. Gordon Tiddy for the stimulating discussion.

References

- 1 D. T. Mitchell, B. W. Ninham and B. A. Pailthorpe, *J. Chem. Soc., Faraday Trans. 2*, 1978, **74**, 1116–1125.
- 2 J. N. Israelachvili, *Intermolecular and Surface Forces*, Academic Press, London, 1992.
- 3 R. G. Horn and J. N. Israelachvili, *J. Chem. Phys.*, 1981, **75**, 1400–1411.
- 4 H. K. Christenson, D. W. R. Gruen, R. G. Horn and J. N. Israelachvili, *J. Chem. Phys.*, 1987, **87**, 1834–1841.
- 5 J. N. Israelachvili and R. M. Pashley, *Nature*, 1983, **306**, 249–250.
- 6 J. Perrin, *Ann. Phys. (Paris)*, 1918, **10**, 160–184.
- 7 J. W. Keuskamp and J. Lyklema, in *Adsorption at Interfaces*, ed. K. L. Mittal, ACS Symposium Series 8, Washington, DC, 1975, pp. 191–198.
- 8 A. D. Nikolov, D. T. Wasan, P. A. Kralchevsky and I. B. Ivanov, in *Ordering and Organisation in Ionic Solutions*, eds. N. Ise and I. Sogami, World Scientific, Singapore, 1988, pp. 302–314.
- 9 A. D. Nikolov and D. T. Wasan, *J. Colloid Interface Sci.*, 1989, **133**, 1–12.
- 10 A. D. Nikolov, P. A. Kralchevsky, I. B. Ivanov and D. T. Wasan, *J. Colloid Interface Sci.*, 1989, **133**, 13–22.
- 11 P. A. Kralchevsky, A. D. Nikolov, D. T. Wasan and I. B. Ivanov, *Langmuir*, 1990, **6**, 1180–1189.
- 12 A. D. Nikolov, D. T. Wasan, N. D. Denkov, P. A. Kralchevsky and I. B. Ivanov, *Prog. Colloid Polym. Sci.*, 1990, **82**, 87–98.
- 13 D. T. Wasan, A. D. Nikolov, P. A. Kralchevsky and I. B. Ivanov, *Colloids Surf.*, 1992, **67**, 139–145.
- 14 V. Bergeron and C. J. Radke, *Langmuir*, 1992, **8**, 3020–3026.
- 15 V. Bergeron, A. I. Jimenez-Laguna and C. J. Radke, *Langmuir*, 1992, **8**, 3027–3032.
- 16 P. Richetti and P. Kékicheff, *Phys. Rev. Lett.*, 1992, **68**, 1951–1954.
- 17 J. L. Parker, P. Richetti, P. Kékicheff and S. Sarman, *Phys. Rev. Lett.*, 1992, **68**, 1955–1958.
- 18 C. E. McNamee, Y. Tsujii, H. Ohshima and M. Matsumoto, *Langmuir*, 2004, **20**, 1953–1962.
- 19 O. Krichevsky and J. Stavans, *Phys. Rev. Lett.*, 1995, **74**, 2752–2755.
- 20 V. Bergeron and C. J. Radke, *Colloid Polym. Sci.*, 1995, **273**, 165–174.
- 21 K. G. Marinova, T. D. Gurkov, T. D. Dimitrova, R. G. Alargova and D. Smith, *Langmuir*, 1998, **14**, 2011–2019.
- 22 E. S. Basheva, A. D. Nikolov, P. A. Kralchevsky, I. B. Ivanov and D. T. Wasan, in *Surfactants in Solution*, ed. K. L. Mittal, Plenum Press, New York, 1991, vol. 11, pp. 467–479.
- 23 E. S. Basheva, K. D. Danov and P. A. Kralchevsky, *Langmuir*, 1997, **13**, 4342–4348.
- 24 G. N. Sethumadhavan, A. D. Nikolov and D. T. Wasan, *J. Colloid Interface Sci.*, 2001, **240**, 105–112.
- 25 K. Koczko, A. D. Nikolov, D. T. Wasan, R. P. Borwankar and A. Gonsalves, *J. Colloid Interface Sci.*, 1996, **178**, 694–702.
- 26 A. Asnacios, A. Espert, A. Colin and D. Langevin, *Phys. Rev. Lett.*, 1997, **78**, 4974–4977.
- 27 V. Bergeron and P. M. Claesson, *Adv. Colloid Interface Sci.*, 2002, **96**, 1–20.
- 28 B. Kolaric, S. Förster and R. von Klitzing, *Prog. Colloid Polym. Sci.*, 2001, **117**, 195–199.
- 29 R. von Klitzing and B. Kolaric, *Tenside Surfactants Deterg.*, 2002, **39**, 247–253.
- 30 C. Stubenrauch and R. von Klitzing, *J. Phys.: Condens. Matter*, 2003, **15**, R1197–R1232.
- 31 C. M. Beltran, S. Guillot and D. Langevin, *Macromolecules*, 2003, **36**, 8506–8512.
- 32 C. M. Beltran and D. Langevin, *Phys. Rev. Lett.*, 2005, **94**, 217803.
- 33 P. Heinig, C. M. Beltran and D. Langevin, *Phys. Rev. E*, 2006, **73**, 051607.
- 34 S. Asakura and F. Oosawa, *J. Chem. Phys.*, 1954, **22**, 1255–1256.
- 35 D. Henderson and M. Lozada-Cassou, *J. Colloid Interface Sci.*, 1986, **114**, 180–183.
- 36 D. Henderson, *J. Colloid Interface Sci.*, 1988, **121**, 486–490.
- 37 R. Kjellander and S. Sarman, *Chem. Phys. Lett.*, 1988, **149**, 102–108.
- 38 P. Attard and J. L. Parker, *J. Phys. Chem.*, 1992, **96**, 5086–5093.
- 39 M. L. Pollard and C. J. Radke, *J. Chem. Phys.*, 1994, **101**, 6979–6991.
- 40 X. L. Chu, A. D. Nikolov and D. T. Wasan, *Langmuir*, 1994, **10**, 4403–4408.
- 41 X. L. Chu, A. D. Nikolov and D. T. Wasan, *J. Chem. Phys.*, 1995, **103**, 6653–6661.
- 42 A. Trokhymchuk, D. Henderson, A. Nikolov and D. T. Wasan, *J. Phys. Chem. B*, 2003, **107**, 3927–3937.
- 43 J. Blawdziewicz and E. Wajnryb, *Europhys. Lett.*, 2005, **71**, 269–275.
- 44 P. A. Kralchevsky and N. D. Denkov, *Chem. Phys. Lett.*, 1995, **240**, 385–392.
- 45 A. Trokhymchuk, D. Henderson, A. Nikolov and D. T. Wasan, *Langmuir*, 2001, **17**, 4940–4947.
- 46 B. H. Zimm, *J. Chem. Phys.*, 1948, **16**, 1093–1099.
- 47 P. A. Kralchevsky, K. D. Danov and N. D. Denkov, in *Handbook of Surface and Colloid Chemistry*, ed. K. S. Birdi, CRC Press, New York, 2002, pp. 137–344.
- 48 M. J. Schick, *Nonionic Surfactants: Surfactant Science Series*, Marcel Dekker, New York, 1987, vol. 23.
- 49 B. Sharma and A. K. Rakshit, *J. Colloid Interface Sci.*, 1988, **129**, 139–144.
- 50 K. S. Sharma, S. R. Patil, A. K. Rakshit, K. Glenn, M. Doiron, R. M. Palepu and P. A. Hassan, *J. Phys. Chem. B*, 2004, **108**, 12804–12812.
- 51 E. D. Manev and R. J. Pugh, *Langmuir*, 1991, **7**, 2253–2260.
- 52 S. Ghosh and S. P. Moulik, *J. Colloid Interface Sci.*, 1998, **208**, 357–366.
- 53 A. Scheludko, *Colloid Polym. Sci.*, 1957, **155**, 39–44.
- 54 A. Scheludko and D. Exerowa, *Colloid Polym. Sci.*, 1959, **165**, 148–151.
- 55 K. J. Mysels and M. N. Jones, *Discuss. Faraday Soc.*, 1966, **42**, 42–50.
- 56 T. D. Dimitrova, F. Leal-Calderon, T. D. Gurkov and B. Campbell, *Langmuir*, 2001, **17**, 8069–8077.
- 57 A. Scheludko, *Adv. Colloid Interface Sci.*, 1967, **1**, 391–464.
- 58 A. S. Dimitrov, P. A. Kralchevsky, A. D. Nikolov and D. T. Wasan, *Colloids Surf.*, 1990, **47**, 299–321.
- 59 N. D. Denkov, H. Yoshimura, K. Nagayama and T. Kouyama, *Phys. Rev. Lett.*, 1996, **76**, 2354–2357.
- 60 N. D. Denkov, H. Yoshimura and K. Nagayama, *Ultramicroscopy*, 1996, **65**, 147–158.
- 61 P. A. Kralchevsky and K. Nagayama, *Particles at Fluid Interfaces and Membranes*, Elsevier, Amsterdam, 2001, ch. 14.
- 62 N. F. Carnahan and K. E. Starling, *J. Chem. Phys.*, 1969, **51**, 635–636.
- 63 H. Reiss, H. L. Frisch, E. Helfand and J. L. Lebowitz, *J. Chem. Phys.*, 1960, **32**, 119–124.
- 64 I. B. Ivanov and B. V. Toshev, *Colloid Polym. Sci.*, 1975, **253**, 593–599.
- 65 G. D. J. Phillies, R. H. Hunt, K. Strang and N. Sushkin, *Langmuir*, 1995, **11**, 3408–3416.
- 66 S. Borbély, *Langmuir*, 2000, **16**, 5540–5545.
- 67 G. Tóth and A. Madarász, *Langmuir*, 2006, **22**, 590–597.
- 68 H. Lange, in *Nonionic Surfactants*, ed. M. J. Schick, Marcel Dekker, New York, 1967, ch. 14, p. 463, Table 14.3.
- 69 M. Rösch, in *Nonionic Surfactants*, ed. M. J. Schick, Marcel Dekker, New York, 1967, p. 760.
- 70 C. Tanford, *The Hydrophobic Effect. The Formation of Micelles and Biological Membranes*, Wiley, New York, 1980, 2nd edn.
- 71 P. C. Hiemenz and R. Rajagopalan, *Principles of Colloid and Surface Chemistry*, Marcel Dekker, New York, 1997, 3rd edn.
- 72 B. V. Derjaguin, *Colloid Polym. Sci.*, 1934, **69**, 155–164.
- 73 T. L. Hill, *An Introduction to Statistical Thermodynamics*, Addison-Wesley, Reading, MA, 1962.
- 74 N. Fuchs, *Z. Phys.*, 1934, **89**, 736–742.
- 75 B. V. Derjaguin, *Theory of Stability of Colloids and Thin Liquid Films*, Plenum Press, New York, 1989.
- 76 W. B. Russel, D. A. Saville and W. R. Schowalter, *Colloidal Dispersions*, Cambridge University Press, Cambridge, 1989.
- 77 G. I. Taylor, personal communication acknowledged by W. Hardy and I. Bircumshaw, *Proc. R. Soc. London, Ser. A*, 1925, **108**, 1–18.
- 78 A. Trokhymchuk, D. Henderson, A. Nikolov and D. T. Wasan, *Langmuir*, 2005, **21**, 10240–10250.
- 79 V. M. Starov, *Adv. Colloid Interface Sci.*, 1992, **39**, 147–174.